Kidney Segmentation from Ultrasound Images using Gradient Vector Force

Arpana M. Kop
Department of Computer Science
Karnatak University
Dharwad, India

Ravindra Hegadi
Department of Computer Science
Karnatak University
Dharwad, India

ABSTRACT
Ultrasonography is said to be the safest technique in medical imaging and is hence used extensively. But the images are noisy with speckle, acoustic noise and other artifacts. The classical segmentation methods fail completely or require post processing step to remove invalid object boundaries in the segmentation results. Problems associated with traditional mode, initialization and poor convergence to concave boundaries of the snakes, however, have limited their utility. A new external force for active contours largely solves both problems. This external force, call gradient vector flow (GVF), is computed as a diffusion of the gradient vectors of a gray-level or binary edge map derived from the image. The resultant field has a large capture range and forces active contours into concave regions. The intensity images are input to the method and a GVF snake is initialized. The snake deforms and finally reveals the contour of the kidney. The proposed method has successfully segmented the kidney part from the ultrasound images.

General Terms
Image processing, medical image analysis.

Keywords
Deformable models, medical image, segmentation, active contours, level sets, GVF.

1. INTRODUCTION
Medical diagnosis seeks information from various sources for proper conclusions on diseases. The sources can be results of clinical tests, patient history, histological reviews, and imaging techniques. Imaging techniques have contributed a lot to the development of medical diagnosis. One such safe and easily available technique is the Ultrasound imaging technique. But the methodology has certain disadvantages, as the images are not very clear and needs an expert to intervene and segment the organ from the image. Moreover, the process takes considerable time for the expert to get the image and to identify the particular part he/she wishes to examine. Further, the process also causes discomfort to the patient. Delay in diagnosis and lack of clarity of image are major issues. A great deal of expertise is needed to get to conclusions using this imaging technique.

The Ultrasound is basic step in the investigation of the disease and is also the safest means of imaging, as the ultrasound waves are less harmful than the other rays used in other methods of medical imaging. Hence it is very commonly used. But, its use is restricted to the expert. Hence, a method for easy recognition of the parts seen through ultrasound imaging device is needed. Research efforts in Image processing techniques have contributed to the developed of Medical Sciences [11]. Researchers have contributed to the improved vision of medical images. A Segmentation method based on active contour without edges is proposed by Dhandra and Ravindra Hegadi [1] in which an endoscopic image is classified as normal or abnormal based on number of regions generated in the image after segmentation. Many research papers on segmentation of kidney region in Ultrasound images have been published using various methodologies in the past.

Bakker et. al. [2] determined the in-vitro kidney volume using an ellipsoidal method in which manual adjustment of an ellipse template was made over the presumed external boundary of the kidney to estimate the volume. Semi-automatic segmentation method was also reported by Matre et. al [3] for in-vitro kidney. In these methods the contour estimation was made for in-vitro kidney, but in real clinical situation the kidney is in-vivo. Classical segmentation methods are fast and useful only for simple and controlled situation. As US kidney images are noisy and have poor signal-to-noise ratio, robust method that makes use of a-priori information to compensate for such difficulty may be used as an alternative. Jun xie et.al. [4] developed a semi-automatic segmentation frame work using both texture and shape priors for kidney contour estimation from noisy Ultrasound image. A novel approach for contour detection of human kidneys from Ultrasound images was also proposed by Marcos Martin-Fernendz et.al. [5]. But these semi-automatic schemes require either a prior knowledge of image in terms of shape and features, which is used to form a smooth contour or need a predefined template for unsupervised deformation. Abouzar Eslami et.al [6] concerned in particular a cystic kidney and developed an automatic approach for renal cyst segmentation from US images. This method is faster and also non-iterative with better accuracy. The semi-automatic or automatic segmentation procedures suggested so far deals with contouring the kidney region by extracting localized features that reflect the region property.

Though the performance of the methods in contouring the kidney region is well appreciated, they fail to formulate a generalized scheme by considering various kidney categories. Unless a common method for contour estimation irrespective of kidney category exists, the implementation of a computer aided diagnosis (CAD) system may not be possible. Mostly the normal kidney images have been considered except where the cystic

This work is supported by the grant under UGC Major Research Project FNO.34-104/2008(SR), Government of India.

kidneys have been taken for implementation. Due to the presence of speckle noise and other constraints establishing the general segmentation scheme for different classes of kidney is difficult and so far not been reported. But efforts of B.Raja et.al [10] have shown the systematic segmentation of kidney using the improved higher order Spline Interpolation method.

In this paper, a reliable semi-automatic segmentation scheme using a Gradient Vector Force is obtained. Uniqueness of this method lies in utilizing the GVF force to deform the initial contour and pull it to fit the actual boundaries of the object. This Paper shows use of the deformable model. There are basically two types of deformable models, parametric deformable models and Geometric deformable models. Under the Parametric deformable models there are again two types one the Energy minimizing formulation and the other is Dynamic force formulation. The two formulations lead to similar results, the first formulation has the advantage that its solution satisfies a minimum principle whereas the second formulation has the flexibility of allowing the use of more general types of external forces. The next section briefly explains the Dynamic Force Formulation using external force GVF that can effectively attract deformable models toward the desired image features.

2. METHODOLOGY

It is convenient to formulate the deformable model [7] directly from a dynamic problem using a force formulation. Such a formulation permits the use of more general types of external forces that are not potential forces, i.e., forces that cannot be written as the negative gradient of potential energy functions [12-15]. According to Newton's second law, the dynamics of a contour $X(s, t)$ must satisfy

$$\mu\frac{\partial^2 X}{\partial t^2} = F_{damp}(X) + F_{\text{int}}(X) + F_{ext}(X)$$

where μ is a coefficient that has a mass unit and F_{damp} is the damping (or viscous) force defined as $-\gamma\partial X/\partial t$, with γ being the damping coefficient. In image segmentation, the mass coefficient μ in front of the inertial term is often set to zero, since the inertial term may cause the contour to pass over the weak edges. The dynamics of the deformable contour without the inertial term becomes

$$\gamma\partial X/\partial t = F_{\text{int}}(X) + F_{ext}(X) \ .$$

The internal forces are:

$$F_{\text{int}}(X) = \frac{\partial}{\partial s}\left(\alpha\frac{\partial X}{\partial s}\right) - \frac{\partial^2}{\partial s^2}\left(\beta\frac{\partial^2 X}{\partial s^2}\right)$$

The External Forces are often expressed as the superposition of several different forces:

$$F_{ext}(X) = F_1(X) + F_2(X) + \ldots + F_N(X),$$

where N is the total number of external forces.

There are several kinds of external forces for deformable models. One of them is the Gradient Vector Flow [8] we shall explain it in this section.

2.1 Parametric deformable models

A traditional snake is a curve x (s) =[$x(s)$, $y(s)$], $s \in [0, 1]$, that moves through the spatial domain of an image to minimize the energy functional

$$E = \int_0^1 \tfrac{1}{2}[\alpha|x'(s)|^2 + \beta|x''(s)|^2] + E_{ext}(x(s))ds \qquad (1)$$

Where α and β weighting parameters that control the snake's tension and rigidity, respectively, and $x'(s)$ and $x''(s)$ denote the

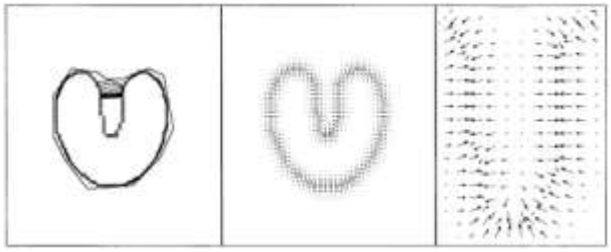

(a) (b) (c)

Figure 1: (a) Convergence of a snake using (b) traditional potential forces, and (c) shown close-up within the boundary concavity.

first and second derivatives of $x(s)$ with respect to s. The external energy function E_{ext} is derived from the image so that it takes on its smaller values at the features of interest, such as boundaries. Given a gray level image $I(x, y)$, viewed as a function of continuous position variables (x, y), typical external energies designed to lead an active contour toward step edges [7] are

$$E_{ext}^{(1)}(x, y) = -|\nabla I(x, y)|^2 \qquad (2)$$

$$E_{ext}^{(2)}(x, y) = -|\nabla[G_\sigma(x, y) * I(x, y)]|^2 \qquad (3)$$

Where $G_\sigma(x, y)$ is a two-dimensional Gaussian function with standard deviation σ and ∇ is the gradient operator. If the image is a line drawing (black on white), then appropriate external energies include [15]:

$$E_{ext}^{(3)}(x, y) = I(x, y) \qquad (4)$$

$$E_{ext}^{(4)}(x, y) = G_\sigma(x, y) * I(x, y). \qquad (5)$$

A snake that minimizes E must satisfy the Euler equation

$$\alpha x''(s) - \beta x''''(s) - \nabla E_{ext} = 0 \ . \qquad (6)$$

This can be viewed as a force balance equation

$$F_{\text{int}} + F_{\text{ext}}^{(p)} = 0 \qquad (7)$$

where $F_{\text{int}} = \alpha x''(s) - \beta x''''(s)$ and $F_{\text{ext}}^{(p)} = -\nabla E_{ext}$. The internal force F_{int} discourages stretching and bending while the external potential force $F_{\text{ext}}^{(p)}$ pulls the snake toward the desired image edges. The snake is made dynamic by treating x as function of

time *t* as well as *s*-i.e., *x*(*s*, *t*). Then, the partial derivative of *x* with respect to *t* is then set equal to the left hand side of (6) as follows:

$$x_t(s,t) = \alpha x''(s,t) - \beta x''''(s,t) - \nabla E_{ext}. \qquad (8)$$

When the solution *x(s, t*) stabilizes, the term $x_t(s,t)$ vanishes and we achieve a solution of (6). A numerical solution to (8) can be found by discretizing the equation and solving the discrete system iteratively.

2.2 Behavior of Traditional Snake

An example of the behavior of a traditional snake is shown in Figure 1. Figure 1(a) shows 64X64 pixel line-drawing of a U-shaped object having a boundary concavity at the top. It also shows a sequence of curves (in black) depicting the iterative progression of a traditional snake (α=0.6 and β= 0.0) initialized outside the object but within the capture range of the potential force field. The potential force field $F_{ext}^{(p)} = -\nabla E_{ext}$ where σ pixel is shown in Figure 1(b). We note that the final solution in Figure 1(a) solves the Euler equations of the snake formulation, but remains split across the concave region. The reason for the poor convergence of this snake is revealed in Figure 1(c), where a close-up of the external force field within the boundary concavity is shown. Although the external forces correctly point toward the object boundary, within the boundary concavity the forces point horizontally in *opposite directions*. Therefore, the active contour is pulled apart toward each of the "fingers" of the U-shape, but not made to progress downward into the concavity. There is no choice of α and β that will correct this problem.

Another key problem with traditional snake formulations, the problem of limited capture range, can be understood by examining Figure 1(b). In this figure, we see that the magnitude of the external forces die out quite rapidly away from the object boundary. Increasing σ in (5) will increase this range, but the boundary localization will become less accurate and distinct, ultimately obliterating the concavity itself when becomes too large. Cohen and Cohen [16] proposed an external force model that significantly increases the capture range of a traditional snake. The performance of a snake using distance potential forces also shows results similar to Figure 1.

This snake also fails to converge to the boundary concavity. This can be seen by inspecting the magnified portion of the distance potential forces which is similar to what is shown in Figure 1(c). We see that, like traditional potential forces, these forces also point horizontally in opposite directions, which pulls the snake apart but not downward into the boundary concavity.

2.3 Gradient Vector Flow Snake

An external potential force generated from the variational formulation of a traditional snake must enter the force balance equation (6) as a static irrotational field, since it is the gradient of a potential function. Therefore, a more general static field $F_{ext}^{(g)}$ can be obtained by allowing the possibility that it comprises both an irrotational component and a solenoidal component.

The overall approach is to use the force balance condition (7) as a starting point for designing a snake. We define below a new static external force field $F_{ext}^{(g)} = v\ (x,\ y)$, which we call the gradient vector flow (*GVF*) field. To obtain the corresponding dynamic snake equation, we replace the potential force $-\nabla E_{ext}$ in (8) with $v(x, y)$, yielding

$$x_t(s,t) = \alpha x''(s,t) - \beta x''''(s,t) + v. \qquad (9)$$

We call the parametric curve solving the above dynamic equation a *GVF snake.* It is solved numerically by discretization and iteration, in identical fashion to the traditional snake.

2.4 Edge map

An edge map $f(x,y)$ derived from the image $I(x,y)$ having the property that it is larger near the image edges. We can use any gray-level or binary edge map defined in the image processing literature for example, we could use

$$f(x, y) = -E_{ext}^{(i)}(x, y) \qquad (10)$$

Where i =1, 2, 3, or 4. Three general properties of edge maps are important in the present context. First, the gradient of an edge map ∇f has vectors pointing toward edges, which are normal to the edges at the edges. Second, these vectors generally have large magnitudes only in the immediate vicinity of the edges. Third, in homogeneous regions, where $I(x,y)$ is nearly constant, ∇f is nearly zero. Because of the first property, a deformable contour initialized close to the edge will converge to a stable configuration near the edge. This is a highly desirable property. Because of the second property, however, the capture range will be very small. Because of the third property, homogeneous regions will have no external forces whatsoever. These undesirable properties can be overcome by extending the gradient map further away from the edges and into homogeneous regions using a computational diffusion process. The inherent competition of the diffusion process will create vectors that point into boundary concavities.

When the gradient of an edge map is used as an external force, because of the first property, a snake initialized close to the edge will converge to a stable configuration near the edge. This is a highly desirable property. Because of the second property, however, the capture range will be very small, in general. Because of the third property, homogeneous regions will have no external forces whatsoever. These last two properties are undesirable. Our approach is to keep the highly desirable property of the gradients near the edges, but to extend the gradient map farther away from the edges and into homogeneous regions using a computational diffusion process. As an important benefit, the inherent competition of the diffusion process will also create vectors that point into boundary concavities.

The Gradient vector flow field is the vector field $v(x, y) = [u(x, y), v(x, y)]$ that minimizes the energy functional

$$\varepsilon = \iint \mu(u_x^{\,2} + u_y^2 + v_x^2 + v_y^2) + |\nabla f|^2 |v - \nabla f|^2 \, dxdy. \qquad (11)$$

This variational formulation follows a standard principle that of making the result smooth when there is no data. In particular, we see that when $|\nabla f|$ is small, the energy is dominated by sum of the squares of the partial derivatives of the vector field, yielding a slowly varying field. On the other hand, when $|\nabla f|$ is large, the second term dominates the integrand, and is minimized by setting $v=\nabla f$. This produces the desired effect of keeping v nearly equal to the gradient of the edge map when it is large, but forcing the field to be slowly-varying in homogeneous regions. The parameter μ is a regularization parameter governing the tradeoff between the first term and the second term in the integrand. This parameter should be set according to the amount of noise present in the image (more noise, increase μ).

Figure 2 (a)

Figure 2(b)

A traditional snake must start close to the boundary and still cannot converge to boundary concavities.

Figure 2 (c)

Figure 2 (d)

A GVF snake can start far from the boundary and will converge to boundary concavities.

Figure 2 (e)

Figure 2 (f)

A GVF snake can even be initialized across the boundaries, a situation that often confounds traditional snakes and balloons.

Using the calculus of variations, it can be shown that the GVF field can be found by solving the following Euler equations

$$\mu\nabla^2 u-(u-f_x)(f_x^2+f_y^2)=0 \qquad (12a)$$

$$\mu\nabla^2 v-(v-f_x)(f_x^2+f_y^2)=0 \qquad (12b)$$

Where ∇^2 is the Laplacian operator. These equations provide further intuition behind the GVF formulation. In a homogeneous region [where $I(x, y)$ is constant], the second term in each equation is zero because the gradient of $f(x, y)$ is zero. Therefore, within such a region, u and v are each determined by Laplace's equation, and the resulting GVF field is interpolated from the region's boundary, reflecting a kind of competition among the boundary vectors. This explains why GVF yields vectors that point into boundary concavities. The numerical implementation and demonstration is given in detail in [8]. Equations (12a) and (12b) can be solved by treating u and v as functions of time and solving

$$u_t(x,y,t)=$$
$$\mu\nabla^2 u(x,y,t)-(u(x,y,t)-f_x(x,y)).(f_x(x,y)^2+f_y(x,y)^2)$$

$$v_t(x,y,t)=$$
$$\mu\nabla^2 v(x,y,t)-(v(x,y,t)-f_y(x,y)).(f_x(x,y)^2+f_y(x,y)^2)$$

The steady solution (as $t \to \infty$) of these linear parabolic equations is the desired solution of the Euler equations (12a) and (12b), which can be further solved as separate scalar partial differential equations in u and v. After computing v(x, y), replacing the potential force $-\nabla E_{ext}$ in the dynamic snake equation as a GVF snake, solved in similar fashion as the traditional snake, (i.e. by discretization and iterative solution), gives us the desired result. Figure 2 shows the movement of the traditional as well as GVF snake. Figure 2(a) shows the deformation of traditional snake. Figure 2(b) shows how traditional, and also other non-GVF, snakes fail to converge to boundary concavities. In figure 2(c) the snake contour is initialized with object of interest within its boundary and the snake contour successfully converged completely over the object when GVF was applied (figure 2(d)). The proposed GVF method could successfully converge even when the snake initialization was done crossing over the object of interest as shown in figure 2(e) and 2(f).

3. RESULTS

The Experimentation is carried out for 5 left kidney and five right kidney ultrasound images. The Gray images of size 256X256 are considered for the proposed segmentation process. Figure 3 (a) shows the original input image containing left kidney. A seed point is selected in the image which lies within the kidney portion of the image and an initial contour is drawn in the form of circle around the seed point as shown in Figure 3 (b). This initial contour will deform by Gradient Vector flow method [1] towards a possible edge of kidney image, as shown in Figure 3 (c). Figure 3 (d) shows the resulting segmented image after 200 iterations. It is found from the experimentation that the edge will arrive to the stability after around 100 iterations. Figure 4 (a) through (d) illustrate the outcome of the segmentation process for another image this time a right kidney. The Kidney boundaries can be seen clearly in the segmented images.

Instance 1

Figure 3 (a): Ultrasound Image of Normal Left Kidney.

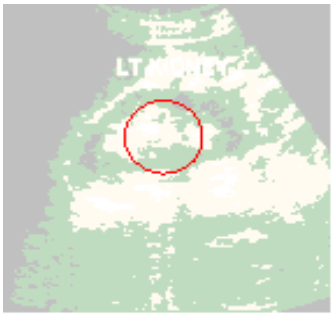

Figure 3 (b): Initial Contour.

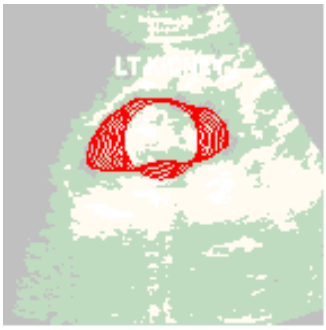

Figure 3 (c): Deformed Snake identifying the Kidney boundaries.

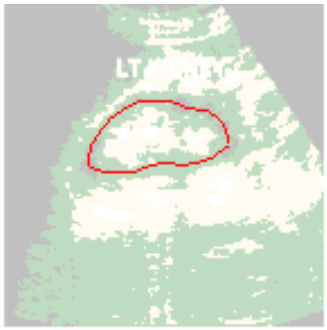

Figure 3 (d): The final contours displaying the segmented kidney.

Instance 2

Figure 4 (a): Image of Normal Right Kidney.

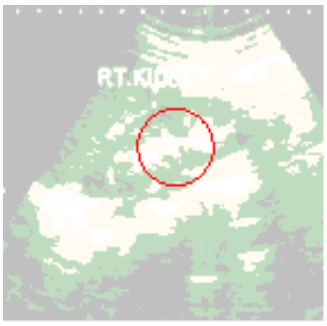

Figure 4 (b): Initial Contour.

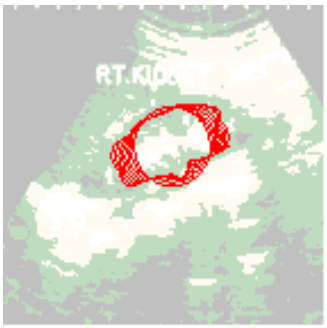

Figure 4 (c): Deformed snake revealing the kidney contour.

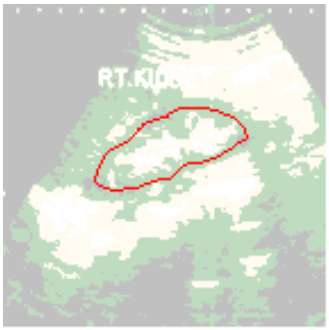

Figure 4 (d): The Final output showing the segmented kidney.

4. CONCLUSION

A method of segmenting kidney from an Ultrasound image has been proposed. The Snakes help to deform the initial contour towards the possible edge of the kidney in Ultrasound images. The experimentation has shown successful segmentation of both left and right kidneys. Based on the segmentation results the kidney size can be estimated. Further experimentation can be

carried out for identification of presence of abnormalities such renal calculus, multi cystic kidney, in these images. Other image features like texture, curvature of the edge and shape of segmented object can be used for better identification and classification.

5. REFERENCES

[1] B. V. Dhandra, Ravindra Hegadi, Mallikarjun Hangarge, V. S. Malemath: Endoscopic image classification based on active contours without edges. ICDIM 2006: 167-172

[2] Bakker, J.,Olree, M., Kaatee, R., de Lange, E.E. and Beek, R.J.A., (1997): 'Invitro Measurement of Kidney Size: Comparison of Ultrasonography and MRI', Ultrasound Med. Biol. 24, pp. 683 – 688.

[3] Matre, K., Stokke, E.M., Martens, D. and Gilja, O.H., (1999): 'Invitro Volume Estimation of Kidneys using 3-D Ultrasonography and a Position Sensor', Eur. J. Ultrasound, 10, pp. 65 – 73.

[4] Jun Xie, Yifeng Jiang and Hung-tat Tsui, (2005): 'Segmentation of Kidney from Ultrasound Images Based on texture and Shape Priors', IEEE Trans. on Medical Imaging, 24 , pp. 45 – 57.

[5] Marcos Martin-Fernandez and Carlos Alberola-Lopez, (2005): 'An Approach for Contour Detection of Human Kidney from Ultrasound Images using Markov Random Fields and Active Contours', Medical Image Analysis, 9, pp. 1 – 23.

[6] Abouzar Eslami, Shohreh Kasaei and Mehran Jahed, (2004): 'Radial Multiscale Cyst Segmentation in Ultrasound Images of Kidney', Proc.4th IEEE International Symposium on Signal Processing and Information Technology, Rome, Italy, pp. 42– 45.

[7] M. Kass, A. Witkin, D. Terzopoulos, "Snakes: Active Contour Models", International Journal of Computer Vision, Vol. 1(4), pp.321-331, 1988.

[8] C. Xu and J. L. Prince, ``Snakes, Shapes, and Gradient Vector Flow," IEEE Transactions on Image Processing, 7(3), pp. 359-369, March 1998.

[9] Nikos Paragois, Olivier Mellina, V.Ramesh, Gradient Vector Flow Fast Geometric Active Contours, IEEE transactions on and Machine Intelligence Volume 26 , Issue 3 (March 2004) : 402 - 407

[10] K Bommanna Raja, M. Madheswaran, K. Thyagarajah, "A General Segmentation scheme for contouring Kidney Region in Ultrasound Kidney Images using improved Higher order Spline Interpolation", 81-88, International Journal of Biological, Biomedical and Medical Sciences, Spring.2007

[11] Tim McInerney, Demetri Terzopoulos, Dept of Computer Science, University of Toronto, Toronto, ON, Canada, "Deformable Models in Medical Image Analysis: A survey", Medical Image Analysis, l (2):91-108, 1996.

[12] C. Xu, A. Yezzi, Jr., and J. L. Prince, "A Summary of Geometric Level-Set Analogues for a General Class of Parametric Active Contour and Surface Models", in Proc. of 2001 IEEE Workshop on Variational and Level Set Methods in Computer Vision (VLSM 2001), pp. 104-111, July 2001.

[13] C. Xu, D. L. Pham, and J. L. Prince, "Medical Image Segmentation Using Deformable Models," SPIE Handbook on Medical Imaging - Volume III: Medical Image Analysis, edited by J.M. Fitzpatrick and M. Sonka, May 2000

[14] C. Xu, D. L. Pham, and J. L. Prince, "Image Segmentation Using Deformable Models", in Handbook of Medical Imaging: Volume 2. Medical Image Processing and Analysis, eds. M. Sonka and J. M. Fitzpatrick, SPIE Press, pp.129-174, 2000.

[15] L. D. Cohen. "On active contour models and balloons". ComputerVision, Graphics, and Image Processing, 53(2):211–218, March1991.

[16] L. D. Cohen and I. Cohen, "Finite-element methods for active contour models and balloons for 2-D and 3-D images," IEEE Trans. Pattern Anal. Machine Intell., vol. 15, pp. 1131–1147, Nov. 1993